PLoRa: A Passive Long-Range Data Network from Ambient LoRa Transmissions

Yao Peng[‡,⋆], Longfei Shangguan[†,⋆], Yue Hu[‡], Yujie Qian[‡]
Xianshang Lin[‡], Xiaojiang Chen[‡], Dingyi Fang[‡], Kyle Jamieson[†]

[†]Princeton University, [‡]Northwest University
⋆: Co-primary authors

ABSTRACT

This paper presents PLoRa, an ambient backscatter design that enables long-range wireless connectivity for batteryless IoT devices. PLoRa takes ambient LoRa transmissions as the excitation signals, conveys data by modulating an excitation signal into a new standard LoRa "chirp" signal, and shifts this new signal to a different LoRa channel to be received at a gateway faraway. PLoRa achieves this by a holistic RF front-end hardware and software design, including a low-power packet detection circuit, a blind chirp modulation algorithm and a low-power energy management circuit. To form a complete ambient LoRa backscatter network, we integrate a light-weight backscatter signal decoding algorithm with a MAC-layer protocol that work together to make coexistence of PLoRa tags and active LoRa nodes possible in the network. We prototype PLoRa on a four-layer printed circuit board, and test it in various outdoor and indoor environments. Our experimental results demonstrate that our prototype PCB PLoRa tag can backscatter an ambient LoRa transmission sent from a nearby LoRa node (20 cm away) to a gateway up to 1.1 km away, and deliver 284 bytes data every 24 minutes indoors, or every 17 minutes outdoors. We also simulate a 28-nm low-power FPGA based prototype whose digital baseband processor achieves 220 μW power consumption.

KEYWORDS

Backscatter, LoRa, Low-power, Long-range

SIGCOMM '18, August 20–25, 2018, Budapest, Hungary

ACM ISBN 978-1-4503-5567-4/18/08…$15.00
https://doi.org/10.1145/3230543.3230567

ACM Reference Format:
Yao Peng[‡,⋆], Longfei Shangguan[†,⋆], Yue Hu[‡], Yujie Qian[‡] Xianshang Lin[‡], Xiaojiang Chen[‡], Dingyi Fang[‡], Kyle Jamieson[†]. 2018. PLoRa: A Passive Long-Range Data Network from Ambient LoRa Transmissions. In *SIGCOMM '18: SIGCOMM 2018, August 20–25, 2018, Budapest, Hungary.* ACM, New York, NY, USA, 14 pages. https://doi.org/10.1145/3230543.3230567

1 INTRODUCTION

The next-generation Internet of Things (IoT) envisions ubiquitous, cheap, and low data-rate connectivity among humans, machines, and objects. A key to this vision is the wireless communication technology that enables extremely impoverished IoT devices to continuously exchange low-rate data. Ideally, such wireless communication should satisfy the following three requirements:

(1) **Battery-free.** IoT devices should be battery-free, purely harvesting energy from the ambient environment and consuming ultra-low power to connect with the gateway.
(2) **Long-range.** IoT devices should be able to communicate over long distances so that those sparsely deployed IoT devices in farms and large warehouses *etc.* can relay data.
(3) **Ambient excitation signal.** IoT devices should use intermittent, ambient IoT signals as their power source and carrier wave, instead of requiring a separate narrowband continuous wave excitation signal, which consistently consumes extra spectrum and complicates deployment.

If the above three requirements were satisfied, we could imagine a pervasively connected world where, for example, a farmer could remotely monitor nutrition levels in a field; a biologist could keep track of wild animal movement, group formulation, population demographics, and prevent poaching incidents; and a warehouse manager could identify every item in the large warehouse without the need to manually inventorying the entire warehouse.

However, to the best of our knowledge, no existing wireless technology satisfies all these three requirements (see Table 1). LoRa [21], NB-IoT [25], and Sigfox [34] enable long-range wireless transmission, yet consume substantial energy. Passive RFID [14, 42] purely harvests energy from the RFID

Table 1: Summary of existing backscatter systems.

Technology	Battery free	Long range	Ambient excitation
Passive RFID [14, 42]	√		
Ambient backscatter [19]	√		√
Turbo charging [28]	√		√
Wi-Fi backscatter [17]	√		√
Passive Wi-Fi [18]	√		
HitchHike [46]			√
FS-Backscatter [49]			√
FM Backscatter [41]	√		√
LoRa backscatter [38]	√	√	
LoRea [40]		√	
FreeRider [48]			√
PLoRa	√	√	√

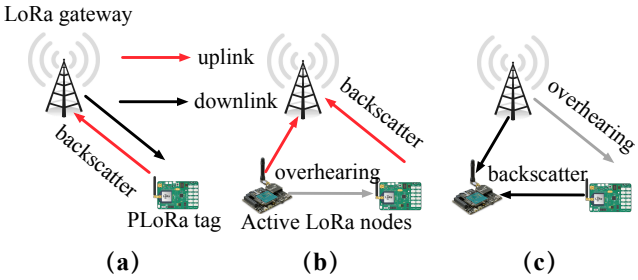

Figure 1: The PLoRa tag (a.) takes downlink LoRa chirps as the excitation signal and modulates them into standard uplink LoRa chirps; (b.) overhears ambient uplink LoRa chirps, using them as excitation to piggyback sensed data to the gateway; and (c.) overhears ambient downlink LoRa chirps, using them as excitation to piggyback sensing data to an active LoRa node in the field.

reader, but only works over a limited range (up to 30 m [7]). LoRa backscatter [38] and LoRea [40] are low-power and long-range, but both require a dedicated continuous wave transmitter to send an excitation signal—a constant sinusoidal tone—as the power source and the carrier for their backscatter transmissions. Deployment of such a special-purposed excitation signal generator increases installation and maintenance costs (due to the need to plug such a device into the electricity grid), and consumes wireless spectrum, especially outdoors or over large geographic areas.

LoRaWAN networks have been successfully deployed in both urban and rural areas for smart city (*e.g.*, smart lighting, air quality monitoring, parking, and vehicle management) and industrial applications (*e.g.*, shipping and transportation, smart farming and livestock management *etc.*) [22]. Gateway and LoRa nodes in these LoRaWAN networks regularly exchange data using chirp-modulated signals that can be decoded at very low signal-to-noise ratio (SNR), thus in principle serving as an excellent excitation signal for long-range backscatter. This observation leads us to propose *PLoRa*, a **P**assive **LoRa** communication technology that enables long-range connectivity for IoT devices based on ambient excitation, without the need for a dedicated excitation source. The PLoRa tag is battery-free, harvests energy from both radio signals and ambient light, and can communicate with both active LoRa nodes and gateways over long distances in three distinct ways (as also shown in Figure 1):

(a) Conventional backscatter. The LoRa gateway directly inquires the PLoRa tag to retrieve its sensor readings. Then the tag uses its low-power electronics to modulate the impedance of its antenna, signaling information back to the gateway at a frequency (uplink) different from the gateway's downlink transmission. The gateway then listens to this frequency and decodes the backscatter data at the same time as the downlink transmission.

(b) Opportunistic uplink piggybacking. An active LoRa node located in proximity to, but not at exactly the same location as the PLoRa tag may transmit its own sensor readings on the uplink to the LoRa gateway. At this time, the PLoRa tag can modulate the active LoRa node's transmission to piggyback its own sensor readings to the gateway. The gateway receives both sensor readings on separate channels (frequencies)—thus the PLoRa tag expands the spatial coverage of the LoRaWAN.

(c) Opportunistic downlink piggybacking. This scenario is the converse of the preceding, with the LoRa gateway transmitting commands to active LoRa nodes on the downlink (*e.g.*, to configure their sensing) but the PLoRa tag may be out of the backscatter range from the LoRa gateway, and so the PLoRa node instead detects the gateway's transmission and uses it to piggyback data to a nearby active LoRa node that is in contact with the gateway. The active LoRa node can then forward these transmissions on to the gateway, resulting in data collection from both node and tag.

In this way, we form a hybrid LoRa network with the existing LoRa infrastructure cooperating with PLoRa nodes to forward data to the gateway in an extensively expanded configuration compared to conventional LoRa networks.

To put this idea into practice, however, there are many significant challenges. First, since the PLoRa tag is battery-free, it should consume an ultra-low amount of power during which it is idle, listening to detect an incoming LoRa packet. The standard LoRa packet detection algorithm first multiplies the incoming signal with a down chirp, then performs an FFT

on the result and searches for FFT peaks. However, generating a down chirp requires the help of a power-hungary digital to analog converter (DAC) and a voltage-controlled oscillator (VCO), thus violating the purpose of using backscatter. Our solution is to reduce the sampling rate of the incoming signals and perform cross correlation for packet detection (§3.1), because power consumption decreases monotonically with the sampling rate.

Second, unlike the sinusoidal tone used in RFID and most other backscatter systems [18, 38, 40], the excitation signal in PLoRa is the normal downlink and uplink LoRa chirps that convey data and change over time. It is thus challenging to modulate this time-varying excitation signal into another standard LoRa chirp for backscatter. Our solution is to let the PLoRa node generate an FSK-modulated baseband signal and multiply it with the incoming LoRa chirp. The multiplication causes a frequency shift of the incoming chirp by $BW/2$ and $-BW/2$, where BW is the LoRa chirp bandwidth. The key observation is that the in-band part of these two shifted chirps, when spliced together, will form a new, standard LoRa chirp (§3.2) that conveys sensing data and is receivable over a long distance.

Third, given the large energy demands of the computational and communication tasks, the battery-free PLoRa tag will soon drain its energy and stop working, which will cause complete loss of data stored in its volatile memory. To solve this challenge, we put forward a holistic energy management hardware design (§4). This hardware works as a finite-state machine to manage the node's state transitions, completing tasks under tight time constraints before energy starvation leads to complete loss of volatile memory, and minimizing energy leakage caused by the static energy consumption of FPGA and sensors on the PCB board when the node is in charging. Our hardware design uses passive components such as resistors, capacitors and low-power active components like switches, and hence is ultra-low power in nature.

Apart from these three core techniques, we also propose a light-weight backscatter signal decoding algorithm (§3.3) and a MAC-layer protocol (§5) to facilitate the coexistence of PLoRa tags and commercial active LoRa nodes in a LoRaWAN. To demonstrate the feasibility of our design, we prototype PLoRa on a four-layer printed circuit board (PCB) using commercial off-the-shelf circuit components and a Microsemi's IGLOO nano low-power FPGA [10] (§6). We evaluate the performance of PLoRa in various indoor and outdoor settings and in different weather conditions. The extensive field studies demonstrate that PLoRa's transmissions can be successfully decoded on the receiver over a distance of 600 m and 1.1 km (depending on the gateway hardware) in outdoor place and cross two concrete walls in an indoor office building, while consuming only 2.591 mW energy in PCB implementation. We also simulate a 28-nm low-power FPGA based prototype whose digital baseband processor consumes 220 μW energy.

Contributions. The primary contributions of this paper are:

- *Proposing a holistic hardware-software co-design to achieve low-power long-range backscatter communication.* The hardware prototype takes an ambient LoRa signal as an excitation signal and employs a novel blind chirp modulation algorithm to transmit data. We further design a low-power current gate circuit to prevent data loss caused by energy depletion.
- *Implementing this hardware-software co-design on the PCB board and evaluating its performance through a long-term (three months) experiment in both indoor and outdoor environment.* Our comprehensive experiments evaluate all three backscatter schemes in various weather conditions including sleet, snow, and clear days.

Limitations. This paper is an early step towards passive long-range data networks, and there is obviously room for continued research. First, PLoRa's packet detection range is limited to 50 m, leaving a large space for improvement. Second, PLoRa's maximum backscatter range is highly sensitive to the power level of the incoming excitation. Third, the LoRa gateway needs to run a dedicated packet reception algorithm for backscatter packet decoding. This is not always feasible due to the limited computation resources on those low-end LoRa gateways. Finally, the current PLoRa design encodes one bit per LoRa symbol and thus achieves a low data rate. Our ongoing work is to improve the performance of four above metrics.

Roadmap. The remainder of this paper first prepares a LoRa primer (§2), then describes PHY-layer (§3), energy management hardware (§4), and MAC-layer design (§5). Our system's implementation (§6) and real-world evaluation (§7) follow. §8 surveys related work. § 9 discusses limitation and future works. §10 concludes.

2 LORA PRIMER

A typical LoRa system consists of two parts: LoRa gateways and LoRa nodes. The LoRa band is divided into multiple uplink and downlink channels: the gateway communicates with LoRa nodes using *downlink* channels, while the LoRa nodes send data to the gateway over *uplink* channels.

LoRa adopts chirp spread spectrum (CSS) modulation, which encodes data using a linear variation of frequency over time. Figure 2 shows a chirp "0" and chirp "1" in the time domain. These two chirps differ from each other in the initial frequency. To demodulate the signal, the receiver performs a FFT on the multiplication of the incoming chirp and a down chirp, whose frequency changes linearly from $BW/2$ to $-BW/2$. This operation leads to a peak in an FFT frequency bin, revealing the time delay of the received chirp.

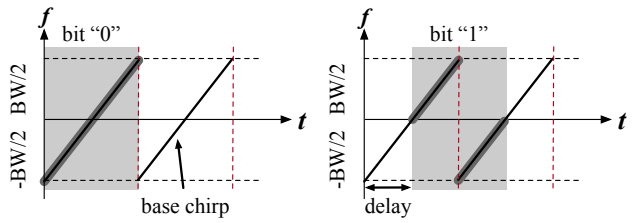

Figure 2: LoRa chirp signal "0" and chirp signal "1": all chirp signals are a slice of a continuous base chirp using an equal-length window (shadowed area), but differing from each other in the initial frequency. BW is the bandwidth.

By tracking the location of the FFT peak, the receiver demodulates the chirp signal. As the chirp fully utilizes its entire allocated bandwidth to encode data, it is more robust to channel noise, Doppler and multi-path effects. The LoRa node changes the spreading factor to control the number of bits encoded in the chirp symbol.

3 PLORA PHYSICAL LAYER

We now describe the PLoRa PHY-layer design including incoming excitation packet detection (§3.1), backscatter signal modulation (§3.2) on the PLoRa tag, and demodulation (§3.3) on the LoRa gateway. We denote the LoRa chirp emitted by the gateway and the active LoRa node as the *active LoRa chirp* and that backscattered by the PLoRa tag as the *passive LoRa chirp*.

3.1 Packet Detection

Conventional backscatter systems [14, 18, 38, 40, 42] omit packet detection on the backscatter tag because the excitation signal they use is a continuous sinusoidal tone sent from a nearby dedicated excitation generator. However in a PLoRa network, the excitation signal is the intermittent LoRa traffic itself, so the PLoRa tag needs to detect this LoRa traffic, synchronize with its LoRa symbols, and use it as the carrier for backscatter. The standard LoRa packet detection algorithm is prohibitive for PLoRa tag due to its substantial energy consumption: it requires a high-power DAC and a VCO, and performs the computation-intensive FFT.

Our approach is to reduce the sampling rate of the incoming signals and perform cross-correlation between these incoming signals and the pre-stored preambles for packet detection and synchronization. It is safe to reduce the sampling rate to some degree because the PLoRa tag does not decode the incoming signals and thus is not restricted by the Nyquist-Shannon sampling theorem. We reduce the sampling rate for packet detection because its power consumption decreases monotonically with the sampling rate [50]. We describe how packet detection works as a signal passes through the circuit shown in Figure 3.

The incoming signal detected by the antenna first goes through an *impedance matching* circuit. We optimize the impedance matching coefficient to ensure that most of the signal power is transferred from the radio wave to the load. After that, the signal passes through a passive band-pass filter (with 20MHz bandwidth), and then is down converted to baseband using an envelope detector. The resulting baseband signal is further digitized with a three-bit low-power ADC. The sampling rate of the ADC is set to S_d/K, far lower than its normal sampling rate S_d = 6 MHz. PLoRa detects the beginning of the preamble by correlating these digital samples with the preamble stored in the FPGA.

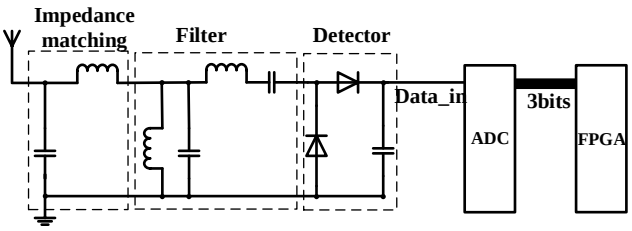

Figure 3: Packet detection workflow on the PLoRa tag.

How to determine the proper sampling rate? Table 2 shows a microbenchmark computing the success rate on packet detection with respect to different K settings. As K increases, the sampling rate decreases, resulting in a lower packet detection success rate but better energy efficiency. Based on this microbenchmark, we find that a good compromise is to set K = 480, yielding a 50 m effective packet detection range (success rate > 99%).

Table 2: The success rate on packet detection in various source-to-tag and sampling rate settings.

Distance (m)	K = 60	120	240	480	960	1920
10	99.7%	99.7	99.7	99.7	78.8	78.8
20	99.7%	99.7	99.7	99.7	78.8	78.8
30	99.7%	99.7	99.7	99.7	75.3	75.3
40	99.7%	99.7	99.7	99.7	78.8	71.0
50	99.7%	99.7	99.7	99.7	78.8	65.4
60	6.65%	6.13	5.11	5.11	3.08	6.15

The low-power FPGA on the PLoRa tag has a limited storage (36 K for the code and data storage) and thus is unable to store the entire preamble of a LoRa packet. We notice that the LoRa preamble is composed of ten identical up chirps (Figure 4). Hence we only need to store one chirp, and correlate it with the incoming signal repeatedly. The tradeoff is slightly higher energy consumption due to frequent memory access.

The detection of ten consecutive up chirps indicates the existence of a LoRa preamble. The FPGA then waits for 2.25 symbol times (the duration for time synchronization) and begins to backscatter. This ensures the PLoRa tag modulates the sensing data onto the payload symbols of the excitation packet. Our microbenchmark (§7.2) shows that such design can successfully detect the LoRa excitation sent from the transmitter 50 m away.

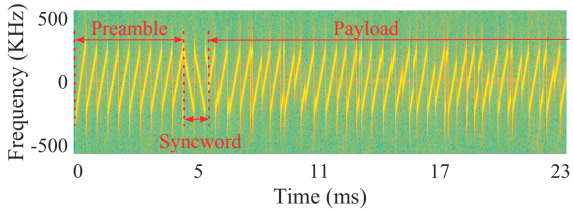

Figure 4: The LoRa packet structure.

3.2 Backscatter Signal Modulation

The PLoRa tag conveys information by modulating the active LoRa chirp into another standard, passive LoRa chirp. This is challenging because the active LoRa chirp (excitation signal) conveys data and changes over time. It is thus difficult to modulate the incoming LoRa chirp into another standard chirp without knowing what the incoming chirp looks like. One possible solution is using ON-OFF keying modulation. However, ON-OFF keying will lead to "broken" LoRa symbols that violate the LoRa standard.

We design a novel *blind chirp modulation algorithm* to solve this challenge. The basic idea is to shift the incoming active LoRa chirp by an amount of $BW/2$ and $-BW/2$, and splice the in-band part of these two shifted LoRa chirps into a new chirp signal. This new chirp occupies the entire allocated bandwidth and thus is a standard LoRa chirp in nature. Compared with ON-OFF keying modulation, this splicing increases the SNR of backscatter signals and thus improves the signal transmission range. The selective frequency shifting could be accomplished with a square wave digital baseband signal [49] that modulates the incoming baseband using Frequency Shift Keying (FSK), setting an FSK mark and space frequency of $BW/2$ and 0, respectively. By switching between these two frequencies at symbol times coinciding with those of the incoming LoRa chirp, the tag could then convey "1" and "0" bits.

Directly applying the foregoing signal mixture causes in-band interference, however, because the generated signal lies in the same channel as the incoming LoRa excitation signal. Note that LoRaWAN standard allocates multiple channels. We thus shift the passive LoRa signal to a different channel, to avoid interference, while at the same time performing the FSK modulation just described.

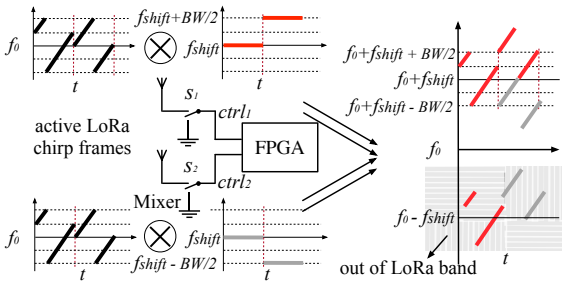

Figure 5: The PLoRa Blind Chirp Modulator: The FPGA generates two frequency plans to control two RF switches separately—these two RF switches shift the passive LoRa signal to another channel for interference avoidance.

To achieve this, the PLoRa tag is designed with two antennas and two switches (mixers) as shown in Figure 5.[1] PLoRa's FPGA generates two frequency plans to control these two RF switches respectively, as shown in the figure. The two RF switches share the same clock and thus are synchronized in time. Specifically, when the node sends a "0" the FPGA generates two identical, time-aligned FSK symbols at frequency f_{shift}, allowing both RF switches to shift the incoming LoRa symbol from the channel centered at f_0 to another channel centered at $f_0 + f_{shift}$. Conversely, if the node sends a "1" the FPGA generates two time-aligned FSK symbols at slightly different frequencies: $f_{shift}+BW/2$ and $f_{shift}-BW/2$. These two frequency plans shift the different part of the incoming LoRa symbol to the new channel centered at $f_0 + f_{shift}$. The in-band part of these two shifted symbols will splice into a new LoRa symbol, which occupies the entire allocated channel. We thus successfully shift the passive LoRa signals to a new channel while at the same time avoiding in-band interference between the active LoRa signal and the passive LoRa signal. On the other hand, the mirror of the passive LoRa signal will be moved out of the LoRa band and thus will not cause interference.

FS-Backscatter [49] uses a ring oscillator to generate the required signal plan for frequency shifting. However, the frequency of the ring oscillator can drift significantly (up to several MHz) with temperature variations outdoors. Therefore in PLoRa, we use the oscillator of a Microsemi IGLOO nano FPGA [10] to generate the required baseband signal directly, which consumes moderately more energy but results in a more stable frequency.

[1] A single-antenna, splitter-combiner based design is also possible, which we leave for future work.

3.3 Backscatter Signal Reception

This section explains how the receiver decodes the passive LoRa signal. Let s_a, s_p, and s_d denote the active LoRa chirp, passive LoRa chirp, and LoRa down chirp, respectively. The receiver receives s_a and s_p and demodulates both.

Basic idea. To demodulate s_p, the receiver performs an FFT twice, the first FFT on the product of s_p and s_d, and the second FFT on the product of s_a and s_d. These two FFT operations will result in two peaks in FFT bins. In essence, these two peaks will fall in the same FFT bin if s_p conveys a "0" bit. Conversely, these two FFT peaks will fall in different FFT bins when a "1" bit is conveyed by s_p, as shown in Figure 6(a). This is because sending a "1" bit will alter the active LoRa chirp (the excitation) s_a into another standard LoRa chirp s_p, as shown in the fifth chirp in Figure 6(b) and Figure 6(c). Hence the receiver can demodulate the backscatter data by examining the location consistency of each pair of FFT bins.

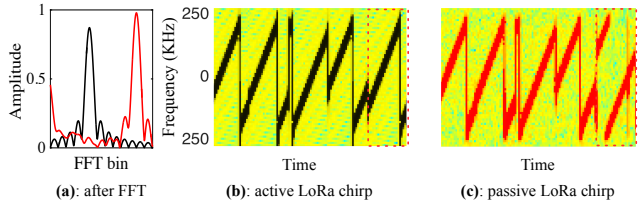

Figure 6: Backscatter signal demodulation: The PLoRa tag sends a 1 bit on the fifth chirp of active LoRa signal, resulting in a new LoRa chirp. These two chirps result in two FFT peaks in different positions.

Accounting for frequency shifting. In reality, however, since clock imprecision exists in the PLoRa tag, the two FFT peaks may not be located exactly in the same FFT bin when the PLoRa node modulates a "0" bit on the excitation. Hence, we demodulate the data y by comparing the location difference of the resulting FFT peaks with a pre-defined threshold:

$$y = \begin{cases} 0, & if \quad |loc_1 - loc_2| \leq threshold, \\ 1, & if \quad |loc_1 - loc_2| > threshold \end{cases}$$

where loc_1 and loc_2 are the locations of the first and the second FFT peak, respectively. We conduct micro-benchmarks in various environments and empirically set the threshold to seven FFT bins (with a 1 KHz FFT bin size), which optimizes the demodulation accuracy.

Packet detection on the receiver. The receiver should be able to detect both the active LoRa packet and the passive LoRa packet before decoding them. The LoRa receiver detects an active LoRa packet using the standard preamble correlation algorithm. However, the receiver cannot detect the passive LoRa packet in the same way because the passive LoRa packet does not have a preamble, as shown in Figure 7. This is because the PLoRa tag does not backscatter signal until it detects the entire preamble of the excitation (§3.1).

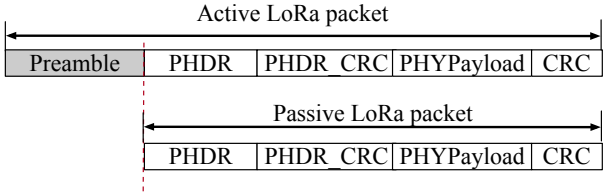

Figure 7: Comparison of packet structure: The backscatter LoRa packet does not have a preamble since it uses the preamble of the excitation signal for packet detection, thus does not reflect it back.

Our passive LoRa packet detection scheme is motivated by the observation that both the active and passive LoRa packets will arrive at the receiver at almost the same time due to the short time difference of transmission of these two packets.[2] Upon detecting the active LoRa packet using the standard correlation algorithm, the receiver locates the beginning of its physical header (PHDR) shown in Figure 7, and sweeps the channels to detect the passive LoRa packet.

4 PLORA ENERGY MANAGEMENT

RF energy harvesting techniques can potentially provide perpetual energy supply to the tag, but are often highly inefficient [23, 26]. Given the large energy demands of computational and communication tasks, without efficient energy management, the tag will soon drain its energy and stop working. We seek a design to manage the node state, switching between charging (energy harvesting) and discharging (backscatter and sensing) at the right moments to prevent data loss due to energy depletion. Finally, our energy management module is designed to be low-power itself.

In PLoRa, we replace the tiny storage capacitor in conventional backscatter systems with a *super capacitor* C_{cap}, as shown in Figure 8. This capacitor has a larger capacity (0.33 F in our system) to provide sufficient energy to activate and operate sensors, and backscatter all sensing data, thus ensuring data integrity. The tradeoff of using a super capacitor is the increased charging time, so we combine RF-based energy harvesting with ambient light-based energy harvesting, improving charging time to 20 minutes (§7.3.3), which satisfies the duty-cycling requirement of most IoT systems [35]. The RF energy harvester harvests energy from all ambient signals on the busy 900 MHz ISM band. To mitigate energy leakage,

[2]This holds in practice since the PLoRa tag should be placed within 50 m from the active LoRa node for excitation packet detection.

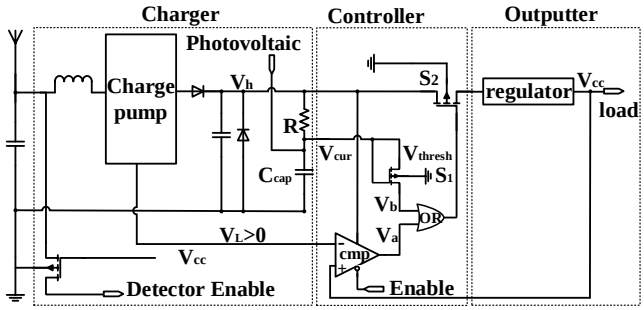

Figure 8: Energy management circuit: The design can be logically divided into three parts: a charger that harvests and stores the energy in the super capacitor, a controller that manages the state transition of the tag, and an outputter that provides voltage supply to enable the tag. The design works independently of the FPGA and consumes only 3.52 μW.

we design a *current gate* to physically cut off circuit connectivity between the energy storage capacitor and all other system components when the PLoRa tag is charging, thus eliminating energy leakage caused by these components.

Hardware design. The energy management circuit design can be divided into three functional modules: a charger, a controller, and an outputter, as shown in Figure 8.

• *Charger.* The role of the charger is to harvest and store the energy in the super capacitor (C_{cap}). The circuit in the figure uses passive components (*e.g.*, resistors, capacitors, and diodes). Hence the charger is ultra-low power in nature.

• *Controller.* The role of the controller is to manage the state transitions of the PLoRa node and prevent energy leakage on the PCB board. It consists of a comparator, an OR gate, and two switches (MOSFET). To save energy, we build our own OR gate using passive components including two diodes and a resistor. These four RF components are low-power, consuming just 3.52 μW in total.

• *Outputter.* The role of the outputter is to provide voltage supply to activate and operate sensors, and backscatter the sensing data to the gateway for further processing. To minimize the energy consumption of the PLoRa tag, we program the regulator to supply a 1.5 V (low) voltage to the tag, thus forcing the tag to work in a low-power mode.

The workflow of this circuit can be described by a finite-state machine, as shown in Figure 9. Each state maintains a circuit condition to control the charging and discharging of the PLoRa tag. Before we describe the state transition details, we first define several parameters for clarity of presentation. Let V_{cur}, V_{thresh}, V_{cc} be the voltage level of the energy storage capacitor, the cut-in voltage of the switch S_1, and the output voltage of the regulator, respectively. V_L and V_H are the lowest-stage and the highest-stage of a five-stage voltage-doubling circuit. V_L is slightly higher than 0 V.

• *From charging state to ready-to-discharge state*: Initially, the super capacitor is empty and so the PLoRa tag stays in the charging state to harvest energy. The voltage level V_b (as shown in Figure 8) of the switch S_1 equals 0 V. Once the capacitor is fully charged (*i.e.*, $V_{cur} > V_{thresh}$), S_1 will be switched on, and thus $V_b = V_{cur}$. Consequently, the OR gate will output a high level to switch on S_2. The energy management module enters ready-to-discharge state.

• *From ready-to-discharge to discharging state*: The regulator outputs a constant voltage V_{cc} = 1.5 V once S_2 is switched on, making the comparator output a high voltage level V_a that in turn keeps S_2 closed. On the other hand, S_1 will be switched off then since V_{cur} will soon drop below the cut-in voltage level of S_1. The energy management circuit then enters discharging state.

• *From discharging state to charging state*: Once the current voltage level of the stored energy V_{cur} drops to a level that is unable to drive the regulator, V_{cc} will drop to 0 V. Accordingly, $V_{cc} < V_L$ and the RF comparator will output a low level voltage signal V_a = 0 V, switching off S_2. The energy management module then goes back to the charging state again, finishing a state transition loop.

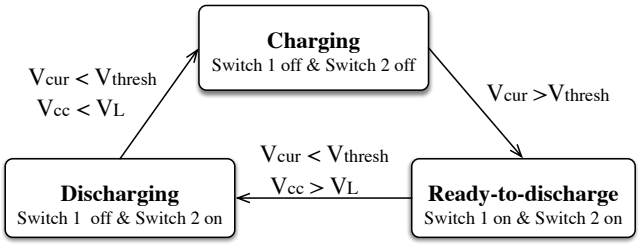

Figure 9: Finite-state machine of the PLoRa's energy management module: The design has three states which the energy management module operate.

Note that during the discharging state, the tag may still have enough energy to drive the regulator after backscattering all sensing data, thus causing unnecessary energy consumption. To avoid this energy waste, the FPGA sends an *enable* signal to the RF comparator each time after backscattering all sensing data, forcing this comparator to switch off S_2, forcing the PLoRa tag into the charging state. It is also worth noting that the switch S_2 physically cuts off the connection between the super capacitor C_{cap} and the regulator when the PLoRa tag is charging. Hence it eliminates the static energy consumption of the FPGA, the RF components, and the sensors on the PCB board, thereby minimizing the energy leakage. Experiments (§7.3.3) show that the current gate improves the charging time over 2.2× and 2.4× indoors

and outdoors, respectively, compared to a design without the current gate.

5 PLORA MAC LAYER

So far we have introduced the physical layer operation and the energy management circuit design of the PLoRa tag. In this section, we describe MAC-layer operation. A typical LoRaWAN consists of multiple active LoRa nodes that abide by the time-domain ALOHA protocol: all LoRa nodes work on the same channel but randomly pick up a time slot to transmit. Multiple PLoRa tags join a LoRaWAN to form a hybrid LoRaWAN network. These PLoRa tags abide by the frequency-domain ALOHA protocol. Upon receiving an excitation, each PLoRa tag randomly shifts the backscatter signal to a different channel, which in turn reduces packet collision rate and improves network scalability.

6 IMPLEMENTATION

We prototype PLoRa tag on a four-layer printed circuit board (PCB) using commercial off-the-shelf circuit components and a Microsemi IGLOO nano AGLE600V2-FG484I FPGA [10] shown in Figure 10(a). The energy harvester consists of a five-stage voltage-doubling amplifier HSMS-286C [9], a photovoltaic charger [45] and a super energy storage capacitor SCDM3R3224 [33]. The transmitter adopts an ADG902 RF switch [2]. We optimize the impedance matching coefficient to provide maximum power transfer from the antenna to the rectifier. The controller of the energy management circuit adopts a low-power voltage comparator NCS2200 [6], an OR gate, and two switches: IR510A [15] (S_1) and 2N7000 [1] (S_2). The PLoRa tag uses two omnidirectional antennas (2 dBi gain) to harvest energy and backscatter signals.

The PLoRa gateway is an NI USRP-2932 software defined radio (SDR) running the modified open source LoRa decoder gr-lora [12]. The USRP uses a single omnidirectional antenna with 2 dBi gain. We set the sampling rate of the USRP to 20 MHz, monitoring six LoRa channels simultaneously. Our decoding algorithm is independent of hardware platform, which can be implemented on a more cost-effective gateway: *e.g.*, a LoRa gateway consisting of a standard Semtech SX1257 LoRa RF-front [36], an IGLOO nano AGLN250V2-VQ100 FPGA [11], and a mini-circuit ZRL-1150LN+ low noise amplifier [20], which cost around $450 in total.

7 EVALUATION

In Section 7.1, we evaluate PLoRa's overall performance in the outdoor Line-of-sight (LoS) and indoor non-line-of-sight (NLoS) scenarios shown in Figure 11. We next conduct microbenchmarks to provide insight into first PLoRa's networking performance (in Section 7.2) and then PLoRa's power management (in Section 7.3).

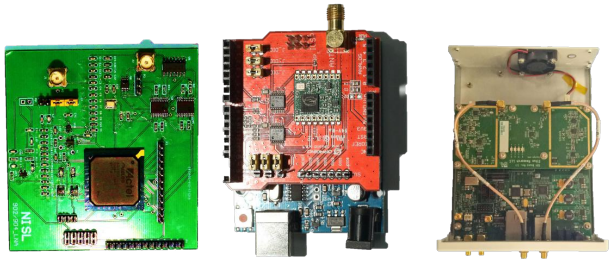

(a): PLoRa tag (b): Active LoRa node (c): USRP-based gateway

Figure 10: Experiment hardware. (a.) PLoRa tag; (b) active LoRa node; (c.) USRP-based gateway. (The photovoltaic charger is separate, and not shown here.)

Experimental setup. Outdoors (Figure 11(a)) we test the PLoRa tag's performance in various weather conditions in an open road. The PLoRa tag harvests energy primarily from the ambient light due to the insufficient RF signals outdoors. For indoor experiments (Figure 11(b)), we put an active LoRa node and a PLoRa tag in the meeting room and move the receiver (gateway) through several adjacent offices to determine the number of walls that the backscatter signal can penetrate. The noise floor in all experiments is around −60 dBm to −70 dBm due to P-GSM-900 cellular interference in the 900 MHz frequency band.[3] The default spreading factor, coding rate, and bandwidth of the ambient LoRa signal is eight, one, and 500 KHz, respectively. As the PLoRa tag will be primarily deployed outdoors, we conduct long-term (three month) experiments to carefully evaluate system performance in various weather conditions (sleet, snow, and clear days). To our best knowledge, this is the first work that comprehensively evaluates ambient long-range backscatter in various environments, with varying weather conditions.

7.1 End-to-End Field Study

In our field study, we ask the following questions: first, what is the maximum backscatter range? Next, how does that range change with bit rate, and how does bit error rate vary with distance? Finally, how does the PLoRa tag perform in its intended setting, a LoRa WAN?

7.1.1 Effective backscatter range. In these experiments, we place one active LoRa node as the excitation signal generator (termed the "source") and evaluate the backscatter range of the PLoRa tag by varying the distance between the source

[3] We expect a longer backscatter range of the PLoRa tag in a relatively clean channel.

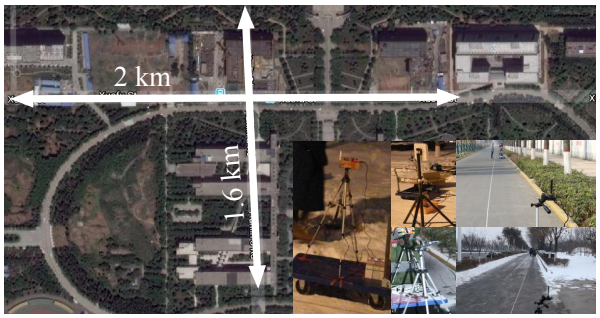

(a) Outdoor line-of-sight experiment map.

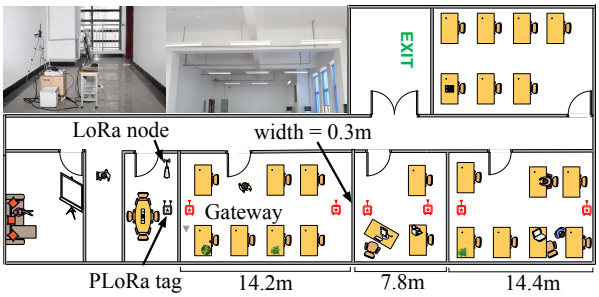

(b) Indoor non-line-of-sight experiment map.

Figure 11: Indoor and outdoor experimental field.

and tag. The experiments are conducted in both outdoor LoS and indoor NLoS environments.

Outdoor scenario. In this experiment, we keep the source stationary and move the PLoRa tag to different locations, searching for the maximum backscatter range; at that limit, we also report packet error rates. We then repeat the measurement for all three backscatter scenarios. The result is shown in Figure 12. When the PLoRa tag is placed near the source (say 20 cm away), it can successfully backscatter the ambient signal to the receiver 600 m away in all three backscatter scenarios. As we increase the tag-to-source distance to 5 m and further to 10 m, the maximum backscatter range decreases to around 200 m and then to around 150 m. We also evaluate maximum backscatter range using a USRP 2954 with better receive sensitivity (−103 dBm versus −88 dBm), and find that the maximum backscatter range jumps to 1.1 km, 1.8× longer than the result achieved by the default USRP 2932 gateway used in our experiments (shown in Table 3). This result highlights the possibility of improving backscatter range by using more sensitive gateway hardware with PLoRa tags.

Table 3: The maximum backscatter range achieved by different gateway hardware.

Device	Sensitivity (dBm)	Backscatter range (m)
USRP 2932	−88	600
USRP 2954	−103	1,100

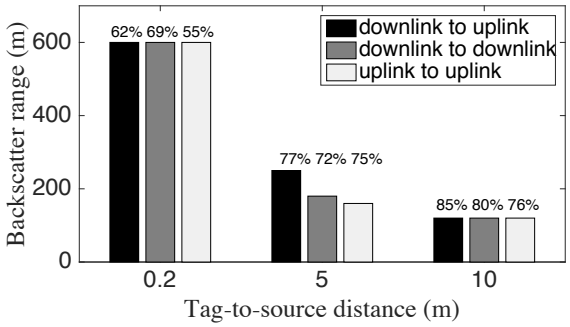

Figure 12: Maximum backscatter range of the PLoRa tag in an outdoor LoS scenario and associated packet loss rate at maximum range (indicated by number above data point).

Indoor scenario. We repeat the previous experiment in an indoor office building and summarize the result in Figure 13. The temperature is 20°C degree. As shown, the signal backscattered by the PLoRa tag can successfully penetrate two concrete walls and be decoded by the receiver 14.4, 16.2, and 17 m away from the PLoRa tag in the three backscatter scenarios, respectively. As we extend the distance between the source and PLoRa tag to 10 m, the backscatter signal becomes much weaker, and thus only penetrate a single concrete wall, arriving at the receiver 8, 8.4, and 8.4 m away in the three backscatter scenarios, respectively.

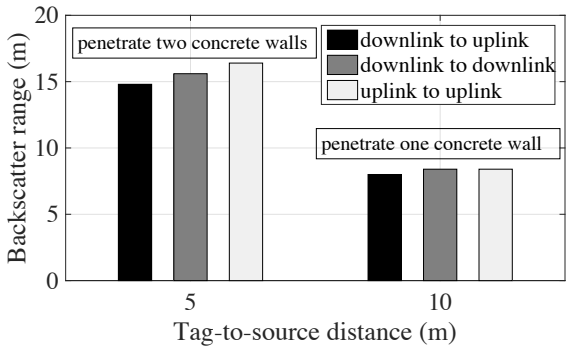

Figure 13: Maximum backscatter range of the PLoRa tag in an indoor office building. The width of the wall is 30 cm. The indoor temperature is 20° C.

7.1.2 Effective backscatter range versus bit rate. Next, we examine the variation of maximum backscatter range with respect to the bit rate. The experiments are conducted outdoors at 5°C degree. One active LoRa node transmits uplink LoRa packets to the gateway at a fixed location. We place a PLoRa tag one meter away from this active LoRa node to backscatter data to the gateway, searching the maximum

backscatter range on different bit rate settings by varying the LoRa spreading factor from seven to 12, corresponding to a bit rate of 6.25, 1.562, 0.781, 0.39, 0.195, and 0.097 Kbit/s, respectively. As shown in Figure 14, the backscatter range increases as we decrease the bit rate. It achieves 300 m at a bit rate of 6.25 Kbit/s. The backscatter range then increases slightly to 500 m when the bit rate decreases to 1.562 Kbit/s, and finally climbs to 800 m when the bit rate is 97 bit/s.

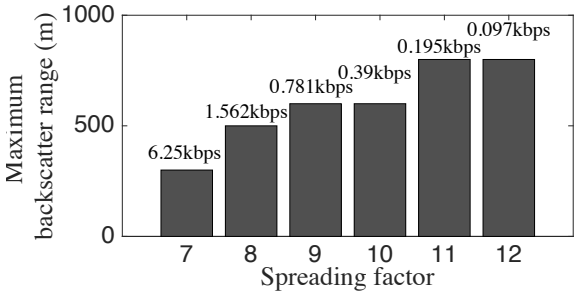

Figure 14: Maximum backscatter range on different bit rate settings. The outdoor temperature is 5° C.

7.1.3 BER at the receiver versus distance. As the PLoRa tag will be primarily deployed outdoors for remote sensing, it is thus important to understand its performance in different outdoor environments. We deploy a simple testbed in an open field outdoors. The PLoRa tag backscatter 100 uplink packets (3300 bit) sent from a nearby active LoRa node to the gateway. We compute the bit error rate (BER) observed at the gateway as a function of distance from the PLoRa tag in three different weather conditions: sleet, cloudy, and sunny. If we do not see any bit errors, we report the BER as 10^{-7}. The result, measured during different weather conditions, is shown in Figure 15. We see that the BER increases with distance in all three weather conditions. This is expected because the backscatter signal experiences a higher attenuation with range, and hence is more susceptible to noise. We also observe that the BER varies significantly across different weather conditions. Specifically, the BER soon jumps to over 0.01 when the gateway is only 138 m away from the PLoRa tag in sleet. In contrast, on a cloudy day the BER is still below 0.01 as we expand the tag-to-gateway distance to 275 m. The PLoRa tag achieves the best performance on a sunny day, where the effective backscatter range exceeds 497 m with a BER lower than 0.01. These results underscore the weather's role on links in LoRa backscatter networks.

7.1.4 PLoRa WAN deployment. We deploy a hybrid PLoRa–LoRa WAN in a 200 × 300 m outdoor field using three active LoRa nodes and a gateway. We then place a PLoRa tag at six random locations in the same field. The PLoRa tag takes the ambient LoRa signals sent from the LoRa nodes and gateway

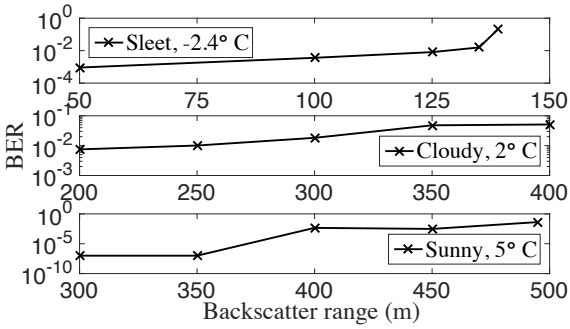

Figure 15: Effective backscatter range in different outdoor environment.

as the excitation signals to modulate its own data. The experiment is conducted on a −5° C degree, snowy day. We show the packet loss rate of both passive and active LoRa packet streams in Figure 16. We see a constant high packet loss rate (over 50%) of both passive and active LoRa packet streams due to the extremely challenging radio environment, which contains strong GSM interference in the 900 MHz RF band as well as the side effect of snow (*cf.* §7.1.3 to see that sleet has a noticeable side effect on a LoRa link). Specifically, we find that the packet loss rate of the passive LoRa stream is just slightly higher than its counterpart over different backscatter range and across all the three backscatter scenarios. This result demonstrates that even in the presence of strong radio interference, the PLoRa tag can achieve competitive performance with an active LoRa node.

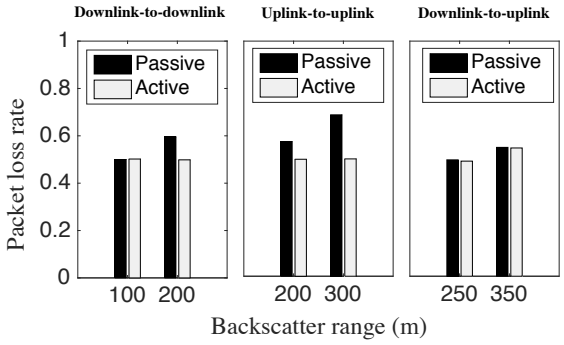

Figure 16: Bit error rate under strong GSM inteference in the 900 MHz ISM band versus backscatter range, for both passive PLoRa and active LoRa packet streams.

7.2 Networking Performance

We now present microbenchmarks that quantify the networking performance of PLoRa's constituent components.

7.2.1 Effective packet detection range. We first study effective packet detection range. We place an active LoRa node

(serving as source) and a PLoRa tag in an indoor corridor shown in Figure 11(b). The active LoRa node sends LoRa signals continuously at a power of 21 dBm. We then move the PLoRa tag to different locations to detect these LoRa signals. As shown in Figure 17, the power (RSS) of the detectable LoRa packet decreases as we move the PLoRa tag away from the source. The maximum packet detection range that the PLoRa tag achieves is 50 m.

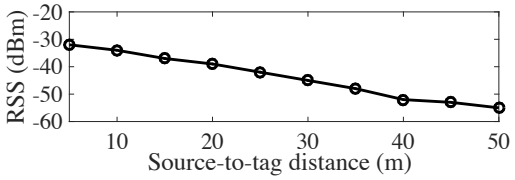

Figure 17: Received signal strength at the PLoRa tag versus distance between excitation source and tag.

7.2.2 Maximum supported workload. Different IoT applications have different requirements on the amount of data to be transmitted. To fulfill these different workload requirements, we examine the maximum number of packets that can be backscattered by the PLoRa tag before draining its energy. We vary the amount of energy stored on the PLoRa tag and measure the total number of packets that are successfully backscattered to the gateway 300 m away until the PLoRa tag consumes up the energy and enters the charging state. Each packet contains 33 payload symbols (*i.e.* 33 bits, or just over four bytes). Table 4 shows that the PLoRa tag can backscatter 69 packets when the tag is fully charged (3.3 V). It then drops slightly to 58, and then to 50 when the energy stored in the super capacitor is 3.1 V and 2.9 V, respectively. As we further decrease the amount of energy stored on the capacity to 2.5 V and 2.3 V, the maximum number of packets that can be backscattered drops to eight and then five, respectively. These different numbers of packets are equivalent to 20 to 284 bytes of information, which is sufficient to send typical sensing data reported by low-power embedded sensors (eight bits per sample). Hence, the PLoRa tag can support sending useful data in various IoT applications.

7.3 Power Consumption

In this section we first present holistic, system-wide power measurements (§7.3.1), followed by a low-power FPGA simulation of the baseband processor (§7.3.2), PCB-based implementation measurements of energy harvesting efficiency (§7.3.3), and implementation-based measurements of the energy management module efficiency (§7.3.4).

7.3.1 System-wide Evaluation. We systematically analyze the power consumption of the PLoRa tag and compare it with the standard LoRa node which consists of a Semtech LoRa SX1257 RF-front [36] and an Arduino uno rev3 board [3], as shown in Table 5. To compute the nominal power consumption of the PLoRa tag and the active LoRa node, we sum the nominal energy consumption of each hardware component listed in the manufacturer's datasheet. For the actual power consumption measurements, we supply a constant 1.5 V to enable the PLoRa tag and the active LoRa node and then use a Keysight U8485A [39] thermocouple power sensor to measure the energy consumption of each functional unit. As expected, the PLoRa tag achieves an order of magnitude lower power consumption than the standard LoRa radio in both packet detection and modulation. PLoRa's energy management module physically cuts off the circuit connection between the energy storage capacitor and the FPGA, the RF components and the sensors on the PCB board, thus eliminating the reported nominal energy consumption of both the packet detection and modulation modules. Total nominal and actual power consumption of PLoRa is 3.5 μW and 2.591 mW, respectively 1000× and 250× smaller than that of a standard LoRa radio.

Table 4: The maximum number of packets that can be backscattered at various energy storage levels.

C_{cap}	3.3 V	3.1 V	2.9 V	2.7 V	2.5 V	2.3 V
# of pkts	69	58	50	31	8	5

Table 5: Nominal (N) and actual (A) power consumption (mW) of the PLoRa tag and an active LoRa node. The active LoRa node does not have an energy management module.

		Pkt. Detect.	Modulation	Energy Mgmt.	Total
PLoRa	N	0	0	0.0035	0.0035
	A	0.144	1.823	0.624	2.591
LoRa	N	3.84	0.33	–	4.17
	A	288	360	–	648

Super capacitor energy leakage. We fully charge the super capacitor of the PLoRa tag and scrutinize its energy leakage by measuring the remaining energy of the tag as a function of time. We shut down the RF harvesting module and conduct the experiment at night to ensure no energy harvesting during the energy leakage measurement. As shown in Figure 18, both the remaining energy and energy leakage rate (the slope of the curve) drops with time. After six hours, the remaining energy of the PLoRa tag is still above the minimum working voltage to power the FPGA, making it possible to recharge again from ambient light, maintaining continuous operation. We believe there is room to further minimize

the energy leakage on the super capacitor by optimizing the hardware circuit design [24].

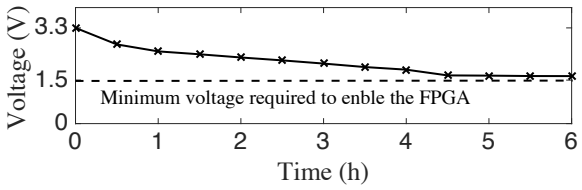

Figure 18: Energy leakage over time.

7.3.2 Low-power FPGA simulation. We simulate the PLoRa digital baseband processor design on a 28 nm low-power FPGA platform, the Xilinx Kintex-7 [44], using the default LoRa spreading factor, coding rate, and bandwidth parameters given above on p. 8. This simulation shows that we can reduce the energy of the baseband processor (the most power-hungry part of the PLoRa tag, listed as **Modulation** in Table 5), to 220 μW. We project an even smaller power consumption in an asynchronous-circuit based ASIC design.

7.3.3 Energy harvesting efficiency. To investigate whether the current gate design can successfully eliminate energy leakage when the tag is charging, we quantify the time required to charge the PLoRa tag to 3.3 V with and without the current gate design in both outdoor (harvesting from the solar and RF signals) and indoor environment (harvesting from fluorescent and RF signals). In the indoor scenario, we put PLoRa tags on a table with a clear LoS to 12 fluorescent lights, evenly spaced on the ceiling of a 16×7 m office, as shown in Figure 11(b), with the tag at a range of 2.6 m to the closest light. In the outdoor scenario, we put PLoRa tags on the ground and let the solar panel face the sun. As shown in Table 6, compared with the PLoRa tag without the current gate design, the PLoRa tag with the current gate design takes less than half of the time to fully charge itself in both indoor and outdoor environment. Specifically, with the current gate module, the PLoRa tag takes only about 24 minutes and 17 minutes to charge from 1.5 V to 3.3 V in an indoor and outdoor environment, respectively. In contrast, if we detach the current gate module, the charging time jumps to 53 minutes and 48 minutes, 2.2× and 2.5× longer than that with the current gate design in the indoor and outdoor case, respectively. This result demonstrates that the current gate can successfully eliminate the energy leakage in the FPGA, backscatter, and sensor components of the system design during charging, thus reducing charging time.

7.3.4 Energy management module efficiency. Table 7 summarizes the nominal energy consumption of the energy management module in WISP 4.0, WISP 5.0, and the PLoRa tag. Both WISP 4.0 and WISP 5.0 require the MCU to manage the state transition, making the total nominal power consumption of the energy management module 5.04 μW and 4.24 μW, respectively. In contrast, the PLoRa tag's energy management works independently from the MCU, controlling state transitions with two switches and a comparator that consumes 30% (1.52 μW) and 17% less energy (0.72 μW) than the WISP 4.0 and 5.0, respectively.

Table 6: Time (minutes:seconds) required to charge the PLoRa tag from various initial energy levels, with/without the current gate design. 1.5 V is the minimum allowable voltage to drive the PLoRa tag.

		1.5 V	1.9 V	2.4 V	2.7 V	3.1 V
Indoor	with	24:05	22:30	18:08	12:26	4:32
	w/o	53:13	49:35	42:27	30:33	12:32
Outdoor	with	17:10	15:14	13:43	9:25	3:37
	w/o	48:02	45:56	38:46	27:00	9:11

Table 7: Nominal energy consumption of the energy management module in PLoRa tag and WISP 5.0.

Platform	Hardware	Energy (μW)
WISP 4.0	MCU, Voltage translator *etc.*	5.04
WISP 5.0	MCU, regulator, power reset	4.24
PLoRa	Comparator, two switches	3.52

8 RELATED WORK

Wi-Fi, TV, and FM backscatter systems. Due to their pervasiveness, Wi-Fi, TV, and FM signals have been extensively exploited for short-range backscatter communication in recent years [4, 17–19, 28, 38, 41, 46, 49]. Ambient Backscatter [19] enables device-to-device communication by backscattering ambient RF signals that conveying TV and cellular data. However, its working range is limited to 0.76 m outdoors and 0.45 m indoors, respectively. With a novel multi-antenna cancellation and coding mechanism design, Turbo charging [28] extends the working range of ambient backscatter to 27 m at a bitrate of 3.33 bps in line-of-sight condition, which is still far away from our goal of ubiquitous wide-area connectivity. Wi-Fi Backscatter [17] exploits existing Wi-Fi infrastructure to provide Internet connectivity to passive devices within a limited working range (2.1 m), BackFi [4] does the same for RFID backscatter, but again within a similar limited range. Passive Wi-Fi [18] enables a passive tag to generate 802.11b transmissions using backscatter communication, but requires a dedicated device to generate excitation signals and works within the limited range of 9 m to 30 m. HitchHike [46] ships data on Wi-Fi packets by translating 802.11b codewords, but the receiver requires two APs

to collaboratively decode the information, which limits its deployment. FS-backscatter [49] designs a low-power ring oscillator (20 μW) to shift Wi-Fi signals to a different channel up to 20 MHz away for collision avoidance. In contrast, PLoRa shifts the signal for both chirp modulation and collision avoidance. FM Backscatter [41] uses ambient FM signals as a source and creates decodable backscatter transmissions on any FM receiver: while an ambient backscatter design, its working range is 1.5–10 m.

Low-power wireless systems. The communication link is among the most power-hungry parts of a typical IoT platform, and various low-power wireless systems have been proposed in the past. Picoradio [30] has pioneered this field, introducing a μW radio design that harvests energy from the solar and transmit data at several bit per second. Bluetooth low energy (BLE) [5] works in the 2.4 GHz band and is widely used in wearable devices, mobiles, and smart home devices. Zigbee [51] is a low-power wireless technology based on IEEE 802.15.4 and designed for local area networks with low-power radios such as wireless sensornets. Both Zigbee and BLE signals are interfered by Wi-Fi transmissions, especially in urban areas where APs are densely deployed. Interscatter [16] backscatters Wi-Fi signals from a Bluetooth excitation signal, but works over Wi-Fi ranges (80 ft.) or less. Sigfox [34] works in the UHF band and transmits PSK modulated data at very low data rate, thus achieving long range like LoRa. NarrowBand IoT (NB-IoT) [25] is designed for connecting a wide range of static IoT devices using cellular telecommunications bands. Among the low-power wireless communication technologies, LoRa is most resilient to both in- and out-of-band interference [37], making it a natural choice for backscatter. LoRa Backscatter [38], introduces a chirp spread spectrum (CSS) backscatter design and harmonic cancellation mechanism to generate a standard LoRa packet that can be decoded by standard LoRa gateway 2 km away. However, it requires a dedicated device to generate a sinusoidal tone as the excitation signal, thus making it less practical for open-field deployment. In contrast, PLoRa does not require a dedicated excitation signal generator, instead exploiting ambient LoRa transmissions. Other work has nearby LoRa nodes transmit a continuous wave excitation signal [29], but again at the expense of their own energy reserves and wireless spectral resources.

Energy management. The energy management modules on many backscatter systems (*e.g.*, WISP [43], Ambient Backscatter [19], Wi-Fi backscatter [17] *etc.*) handle state transitions but don't ensure data integrity. Furthermore, these systems enter the charging state after energy depletion, but still keep the circuit connection between the energy storage capacitor and the regulator, causing substantial energy leakage. To maintain data integrity, Mementos [31] adopts a checkpoint design to save program instructions or data to nonvolatile memory when energy is about to run out. However, Mementos needs to frequently sample the voltage level of the capacitor, which increases the CPU workload and thus is not energy-efficient. QuarkNet [47] segments a data frame into smaller micro-frames with various sizes depending on the prevailing energy harvesting conditions, thus ensuring the data integrity of each transmitted frame. PLoRa, on the other hand, adopts a hardware-based solution using a super-capacitor coupled with highly efficient energy management hardware, to achieve the same end.

9 DISCUSSION

Improving packet detection range. The maximum packet detection range of the PLoRa tag is 50 m. This range can be further improved by leveraging the advanced envelope detector design [27, 32]. For example, the state-of-the-art envelope detector achieves -71 dBm sensitivity [13], translating to 565 m effective packet detection range based on an open-field experiment. We leave this as future work.

Out-of-band LoRa signal interference. The tag's envelope detector essentially captures energy from all LoRa channels and hence is unable to detect incoming excitation when multiple LoRa nodes transmit on different channels at the same time. However, this rarely happens in practice since many LoRa nodes typically transmit on the same channel in a typical LoRaWAN network [8].

Large-scale deployment. Our current evaluation results are based on a small testbed with one PLoRa tag and three active LoRa nodes. As more PLoRa tags join the network, packet collision rate will inherently increase. Our future plan is to deploy a larger hybrid LoRa testbed outdoors with tens of active LoRa nodes and PLoRa tags, examining the robustness of PLoRa's design.

10 CONCLUSION

PLoRa is an ambient, passive LoRa backscatter design that provides low-power and long-range connectivity for IoT devices. Our design combines a low-power packet detection circuit with novel blind chirp modulation and harmonic cancellation techniques. Our PCB prototype can backscatter to a LoRa gateway up to 1.1 km away and deliver 284 bytes of sensor data with a 17 minute duty cycle.

ACKNOWLEDGEMENTS

We thank our shepherd Prof. Fadel Adib and the anonymous reviewers for their constructive feedback. This work is supported by NSF Awards #1617161 and #1763309, NSFC Awards #61772422 and #61672428.

REFERENCES

[1] 2N7000 MOSFET. Website.
[2] ADG902 RF switch. Website.
[3] Arduino uno rev3. Website.
[4] D. Bharadia, K. R. Joshi, M. Kotaru, S. Katti. BackFi: High throughput Wi-Fi backscatter. *SIGCOMM Comput. Commun. Rev.*, **45**(4), 283–296, 2015.
[5] Bluetooth low energy. Website.
[6] NCS2200 Series, NCS2200A Low Voltage Comparators. Website.
[7] D. M. Dobkin. *The RF in RFID: UHF RFID in practice.* Newnes, 2012.
[8] A. Dongare, R. Narayanan, A. Gadre, A. Luong, A. Balanuta, S. Kumar, B. Iannucci, A. Rowe. Charm: Exploiting geographical diversity through coherent combining in low-power wide-area networks. *IPSN*, 2018.
[9] Surface Mount Microwave Schottky Detector Diodes. Website.
[10] IGLOO nano FPGAs. Website.
[11] Microsemi Corporation AGLN250V2-VQ100 FPGA. .
[12] gr-lora decoder. Website.
[13] C. Hambeck, S. Mahlknecht, T. Herndl. A 2.4 μw wake-up receiver for wireless sensor nodes with- 71dbm sensitivity. *Circuits and Systems (ISCAS), 2011 IEEE International Symposium on*, 2011.
[14] P. Hu, P. Zhang, D. Ganesan. Laissez-faire: Fully asymmetric backscatter communication. *SIGCOMM*, 2015.
[15] IR510A MOSFET. Website.
[16] V. Iyer, V. Talla, B. Kellogg, S. Gollakota, J. Smith. Inter-technology backscatter: Towards internet connectivity for implanted devices. *SIGCOMM*, 2016.
[17] B. Kellogg, A. Parks, S. Gollakota, J. R. Smith, D. Wetherall. Wi-Fi backscatter: Internet connectivity for RF-powered devices. *SIGCOMM*, 2014.
[18] B. Kellogg, V. Talla, S. Gollakota, J. R. Smith. Passive Wi-Fi: Bringing Low Power to Wi-Fi Transmissions. *NSDI*, 2016.
[19] V. Liu, A. Parks, V. Talla, S. Gollakota, D. Wetherall, J. R. Smith. Ambient backscatter: wireless communication out of thin air. *SIGCOMM*, 2013.
[20] Mini-circuit ZRL-1150LN+ low noise amplifier. .
[21] LoRa. Website.
[22] Four-faith LoRa application. Website.
[23] C. Lu, V. Raghunathan, K. Roy. Efficient design of micro-scale energy harvesting systems. *IEEE Journal on Emerging and Selected Topics in Circuits and Systems*, 2011.
[24] S. Naderiparizi, A. N. Parks, Z. Kapetanovic, B. Ransford, J. R. Smith. Wispcam: A battery-free rfid camera. *RFID*, 2015.
[25] Narrow-band IoT. Website.
[26] P. Nintanavongsa, U. Muncuk, D. R. Lewis, K. R. Chowdhury. Design optimization and implementation for RF energy harvesting circuits. *IEEE Journal on emerging and selected topics in circuits and systems*, 2012.
[27] S. Oh, N. E. Roberts, D. D. Wentzloff. A 116nw multi-band wake-up receiver with 31-bit correlator and interference rejection. *CICC, 2013 IEEE*, 2013.
[28] A. N. Parks, A. Liu, S. Gollakota, J. R. Smith. Turbocharging ambient backscatter communication. *SIGCOMM*, 2015.
[29] C. Pérez-Penichet, F. Hermans, A. Varshney, T. Voight. Augmenting IoT networks with backscatter-enabled passive sensor tags. *HotWireless*, 2016.
[30] J. M. Rabaey, M. J. Ammer, J. L. da Silva, D. Patel, S. Roundy. Picoradio supports ad hoc ultra-low power wireless networking. *Computer*, **33**(7), 42–48, 2000.
[31] B. Ransford, J. Sorber, K. Fu. Mementos: System support for long-running computation on RFID-scale devices. *ACM SIGPLAN Notices*, 2012.
[32] N. E. Roberts, D. D. Wentzloff. Ultra-low power wake-up radios. *Ultra-Low-Power Short-Range Radios*, 137–162, 2015.
[33] Samwha Tech Corp. SCDM3R3224 super capacitor. Website.
[34] Sigfox. Website.
[35] LoRa Technology Is Connecting Our Smart Planet. Website.
[36] Semtech SX1257. Website.
[37] Semtech SX1276 Transceiver. Website.
[38] V. Talla, M. Hessar, B. Kellogg, A. Najafi, J. R. Smith, S. Gollakota. LoRa Backscatter: Enabling The Vision of Ubiquitous Connectivity. *IMWUT*, 2017.
[39] U8485A DC/10 MHz–33 GHz USB Thermocouple Power Sensor. Website.
[40] A. Varshney, O. Harms, C. Pérez-Penichet, C. Rohner, F. Hermans, T. Voigt. Lorea: A backsca er architecture that achieves a long communication range. *SenSys*, 2017.
[41] A. Wang, V. Iyer, V. Talla, J. R. Smith, S. Gollakota. FM Backscatter: Enabling Connected Cities and Smart Fabrics. *NSDI*, 2017.
[42] J. Wang, H. Hassanieh, D. Katabi, P. Indyk. Efficient and reliable low-power backscatter networks. *SIGCOMM*, 2012.
[43] Intel WISP 4.0. Website.
[44] Xilinx kintex 7 datasheet. Website.
[45] Photovoltaic Charger XRYG-905. Website.
[46] P. Zhang, D. Bharadia, K. R. Joshi, S. Katti. HitchHike: Practical Backscatter Using Commodity WiFi. *SenSys*, 2016.
[47] P. Zhang, D. Ganesan. Enabling bit-by-bit backscatter communication in severe energy harvesting environments. *NSDI*, 2014.
[48] P. Zhang, C. Josephson, D. Bharadia, S. Katti. Freerider: Backscatter communication using commodity radios. *CoNEXT*, 2017.
[49] P. Zhang, M. Rostami, P. Hu, D. Ganesan. Enabling practical backscatter communication for on-body sensors. *SIGCOMM*, 2016.
[50] X. Zhang, K. G. Shin. E-mili: Energy-minimizing idle listening in wireless networks. *IEEE Transactions on Mobile Computing*, 2012.
[51] Zigbee. Website.